ACS Catalysis

pubs.acs.org/acscatalysis Research Article

Boron-Induced Redispersion of Pt Species during Propane Dehydrogenation

Mengyang Liu,[‖] Shaobo Han,[‖] Wenna Zhang,[‖] Bin Gu,* Jingmei Li, Huangzhao Wei, Xin Rong, and Chenglin Sun*

Cite This: *ACS Catal.* 2025, 15, 4251−4258 Read Online

ACCESS | Metrics & More | Article Recommendations | Supporting Information

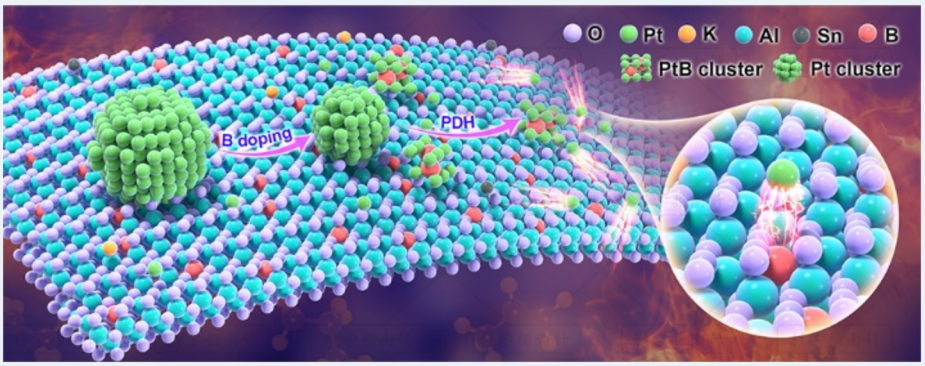

ABSTRACT: In a propane dehydrogenation (PDH) reaction system, low-Pt catalysts generally suffer from rapid deactivation and poor durability due to easy sintering at high temperatures and in a reductive atmosphere. Herein, we develop a catalyst (PtSnK-B/Al_2O_3, named as PtSnK-B0.32) with both low Pt loading (0.15 wt %) and high durability by facile doping of trace boron into a conventional Pt-based catalyst. Density functional theory (DFT) calculations show that pure Pt clusters have weak binding energy with support, leading to a further undesired Pt sintering process. In contrast, when boron (B) is added to the Pt-based catalyst, the undesired Pt sintering process is significantly inhibited. Moreover, being initiated by propane molecules, the pure Pt clusters are readily to dissociate into Pt atoms due to their longer Pt-Pt bond lengths, then the dissociated Pt atoms are captured by B or BO_x species to form stable Pt−B clusters under PDH conditions. The formation of highly dispersed Pt−B clusters allows the catalyst to achieve high intrinsic activity; compared with the catalyst without B (PtSnK, 0.14 wt % Pt), the E_a value of the B-doped catalyst is obviously reduced. Significantly, the durability of PtSnK-B0.32 is three times that of PtSnK and even twice that of 0.26PtSnK with a Pt loading of 0.26 wt %. The facile synthesis method, lower Pt content, and higher durability provide a promising application perspective.

KEYWORDS: *propane dehydrogenation, low Pt loading, antisintering, redispersion, high durability*

1. INTRODUCTION

PDH process has attracted increasing interest because of the outburst of shale gas and growing demand for propylene to produce valuable chemicals, such as polypropylene, epoxypropane, and phenol/acetone.[1−3] Pt(-Sn)/Al_2O_3 is the most widely used catalyst in the Oleflex PDH process. However, PDH is industrially operated at 570−650 °C as it is a strong endothermic process (ΔH_{298}^{θ} = 124.3 kJ mol^{-1}).[1,4,5] Catalysts exposed to a reductive atmosphere at such high temperatures suffer from severe Pt sintering, resulting in fast catalyst deactivation.[6,7] Therefore, a high content of precious Pt (approximately 0.3 wt %) is required for achieving reasonable propylene yield, leading to increased catalyst cost. Moreover, frequent regeneration for deactivated catalysts is necessary, where highly toxic Cl_2 is used to redisperse Pt species through an oxychlorination reaction.[8,9] Developing a catalyst with high Pt dispersion and sintering resistance is an ultimate target for the PDH industry.

Enhancing metal−support interfacial bonding has been proven effective to improve Pt dispersion.[10,11] Pt species can be highly dispersed on $Al_{(V)}$-abundant Al_2O_3 nanosheets through Pt−$Al_{(V)}$ interactions, but Pt aggregation is unavoidable as the proceeding of PDH.[12] The Pt−Sn/CeO_2 catalyst, with Pt atoms strongly trapped on ceria, relies on frequent regeneration to achieve redispersion.[8] Although aggregation of

Received: November 24, 2024
Revised: February 18, 2025
Accepted: February 19, 2025
Published: February 24, 2025

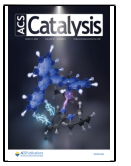

Pt single atoms on isolated CeO_x nanoglues islands ($Pt/CeO_x/SiO_2$) is inhibited when each CeO_x nanocluster hosts less than one Pt atom, precise control of electrostatic adsorption strategy is necessary, and isolated Pt atoms on CeO_2 have been proved to be less selective to propylene.[8,13]

Alloying Pt with transition metals (Sn,[14] Zn,[15,16] Ga,[17] In,[18,19] and Cu[20]) is an effective strategy to maintain high Pt dispersion and low Pt usage by physical isolation or partial coverage. Zn-based catalyst with high PDH activity has been achieved by modification with trace platinum (0.1 wt %).[21] Additionally, Pt−Cu single atom alloys and [$PtZn_4$] intermetallic alloys with 0.1 wt % Pt loading have been established.[15] These geometry-isolated and electron-rich Pt sites in alloys readily promote the cleavage of the first and second C−H bonds of propane but inhibit the deep dehydrogenation of propylene. Moreover, a 0.1 wt % Pt catalyst is proposed by silica coating, which changes the interface between $PtGa/Al_2O_3$ and SiO_2, forming immobilized Ga oxide clusters and tightly anchored Pt catalytic sites.[3] However, these low-Pt catalysts generally suffer from rapid deactivation and poor durability due to easy sintering. As of now, the exploration of PDH catalysts with low Pt content, high Pt dispersion, and enhanced durability remains challenging.

Here, we report a low-Pt (0.15 wt %) catalyst with both excellent catalytic activity and durability by doping a trace amount of B into conventional $Pt−Sn−K/Al_2O_3$-based catalyst. On a B-doped catalyst, the undesired Pt sintering process is significantly inhibited, and Pt species are redispersed during PDH, showing benign sintering resistance. This work provides a practically feasible approach to less regeneration frequency, higher production, and lower costs simultaneously for the PDH industry.

2. METHODS

2.1. Synthesis of Catalysts. A B-doped catalyst was prepared via an incipient-wetness impregnation method. In detail, spherical θ-Al_2O_3 support (1.4−1.6 mm, S_{BET} = 107 m^2/g) was impregnated with a solution containing theoretical amounts of H_2PtCl_6, $SnCl_2$, KCl, and H_3BO_3, followed by drying at 120 °C and calcination in stagnant air at 520 °C for 4 h. The calcined catalyst was reduced under a H_2 flow at 600 °C for 2 h. The theoretical loadings of Pt, Sn, B, and K were 0.15, 0.1, 0.15, 0.35, and 0.65 wt %, respectively. The B-doped catalysts were labeled as PtSnK-B*x*, where *x* refers to their actual B loading. Similarly, catalysts without B were also prepared using the same procedure and labeled as PtSnK.

2.2. Characterizations. X-ray diffraction (XRD) measurements were performed at room temperature on a Panalytical X'Pert PRO Powder X-ray diffractometer with a Cu Kα source (λ = 1.5406 Å); the current and voltage were 40 kV and 40 mA, respectively. Nitrogen physisorption was measured with a NOVAe adsorption analyzer (Quantachrome). Before the measurements, samples were degassed at 300 °C for 5 h. The specific surface areas (S_{BET}) were calculated from adsorption data in the relative pressure range of 0.05−0.3 using the Brunauer−Emmett−Teller (BET) method. Pore size distribution was calculated using the Barrett−Joyner−Halenda (BJH) pore size model. The actual loading of Pt and B in fresh and used catalysts were determined by inductively coupled plasma optical emission spectroscopy (ICP-OES, 7300DV, PerkinElmer). AC-HAADF-STEM images were obtained with a JEM-ARM200F microscope (JEOL) operated at 200 kV and equipped with a cold-field-emission gun, which can achieve a resolution of 0.07 nm. The samples were prepared by dropping an ethanol droplet of the samples onto carbon-coated copper grids and drying at room temperature. The CO−DRIFT spectra were recorded on a VERTEX 80 V full-band high-resolution infrared spectrometer (Bruker). After being loaded in the Harrick diffuse reflector, the sample was heated to 300 °C for 1 h in helium to remove adsorbed water and cooled to 30 °C. The CO−DRIFT spectra before 1%CO/He exposure were recorded. Then, the samples were exposed to 1%CO/He flow (50 mL min^{-1}) for 35 min followed by purging with He flow (50 mL min^{-1}) for 35 min to ensure that the surface of Pt species was fully saturated with CO. Then, the CO−DRIFT spectra after 1%CO/He exposure were recorded. Then, CO−DRIFT spectra were obtained by subtracting the spectra collected after and before exposure to 1%CO/He. The spectra were recorded by collecting 64 scans at a resolution of 4 cm^{-1}. H_2-TPR was measured on a Micromeritics AutoChem II 2920 instrument. Typically, 100 mg of samples were employed for each measurement. The sample was pretreated at 300 °C in Ar gas flow for 1 h and then cooled to 25 °C under Ar. Subsequently, the sample was heated to 800 °C under 10% H_2−Ar gas flow, and the H_2 consumption was monitored by a thermal conductivity detector (TCD). Synchrotron radiation experiments were performed at BL11B of Shanghai Synchrotron Radiation Facility (SSRF) (Shanghai, China) and Singapore Synchrotron Light Source (SSLS) center. The Pt L_{III}-edge extended X-ray absorption fine structure (EXAFS) spectra were recorded in transmission mode at room temperature using a four-channel Silicon Drift Detector (SDD) Bruker 5040. The samples were calibrated using standard Pt foil, which was simultaneously measured as a reference. All of the analyses (including data reduction, data analysis, and EXAFS fitting) were performed with the Athena and Artemis software. For EXAFS modeling, EXAFS of the Pt foil was fitted, and the obtained amplitude reduction factor S_0^2 value (0.816) was set in the EXAFS analysis to determine the coordination numbers (CNs) for the Pt−O/B/Pt scattering paths in the samples.

2.3. DFT Calculation. All DFT calculations were performed with the Perdew−Burke−Ernzerhof (PBE) functional using the Vienna Ab initio Simulation Package (VASP).[1] The projector amplified wave (PAW) method was employed to describe the core−valence electron interactions. A 2 × 2 × 1 γ grid of *k*-points was used for Brillouin zone integration. The valence electronic states were expanded in the plane-wave basis sets with an energy cutoff of 500 eV. A Gaussian smearing of 0.05 eV was applied during geometry optimization. The convergence criteria for the iteration in the self-consistent field (SCF) were set at 10^{-5} eV, and the residual force for optimizing atom positions was constrained to less than 0.02 eV/Å. The Al_2O_3(010) surface and Pt(111) are chosen as the exposed surface for calculations.

2.4. Propane Dehydrogenation Tests. The propane dehydrogenation reaction was carried out under atmospheric pressure in a quartz tube reactor with an inner diameter of 18 mm. Propane flow with a H_2:C_3H_8 molar ratio of 0.5:1 was passed through 1.0 g of spherical catalyst at 600 °C, with a weight hourly space velocity (WHSV) of 3.04/10.6/21.2 h^{-1}. The gas product was analyzed using an online Agilent 7890A gas chromatograph equipped with an FID detector and HP-Al_2O_3/KCl capillary column. Catalyst lifetime experiments were carried out in a stainless reactor with 6 g of catalysts. The

https://doi.org/10.1021/acscatal.4c07243
ACS Catal. 2025, 15, 4251−4258

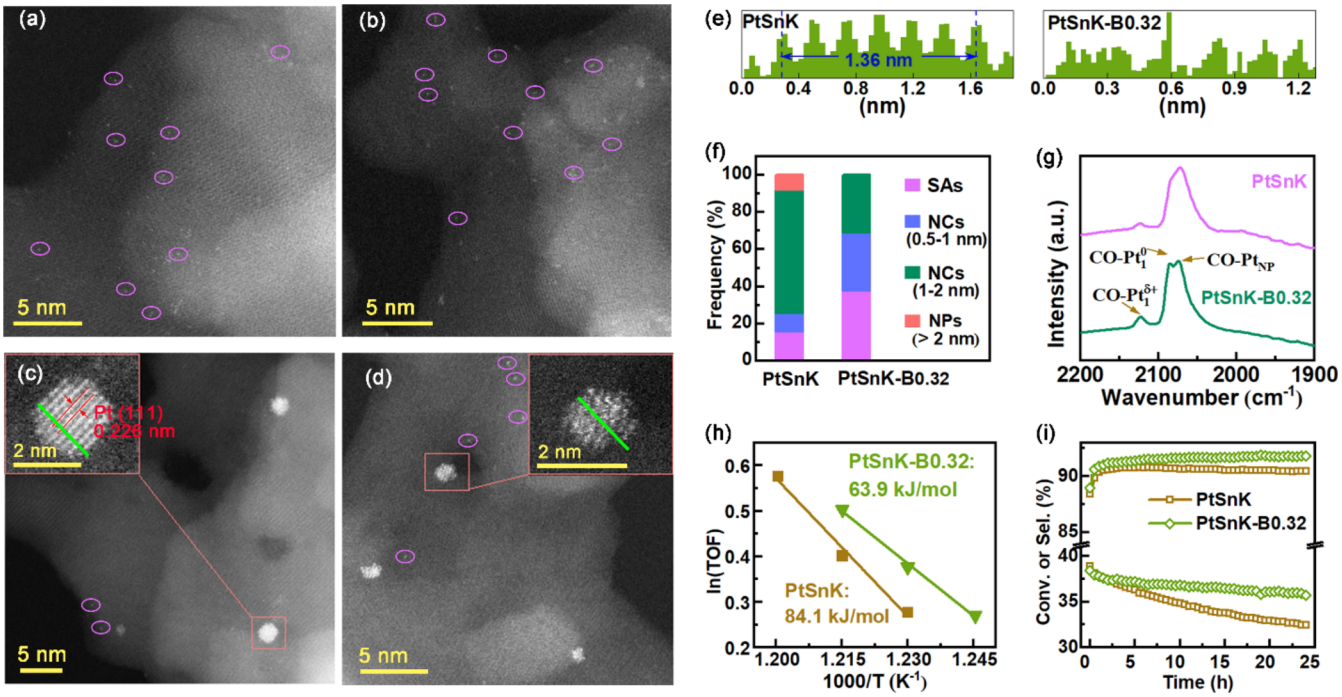

Figure 1. AC-HAADF-STEM images of as-calcined PtSnK (a) and PtSnK-B0.32 (b) at 520 °C for 4 h, and as-reduced PtSnK (c) and PtSnK-B0.32 (d) under pure H_2 flow for 2 h. (e) Crystal lattice fringe of as-reduced PtSnK and PtSnK-B0.32 along green lines in (c, d). (f) The histogram of the size distribution of Pt species for as-reduced PtSnK and PtSnK-B0.32 under H_2 (more than 200 counts for each catalyst). (g) CO−DRIFTS of PtSnK and PtSnK-B0.32. (h) Arrhenius plots of catalysts, reaction condition: 25 mg of catalyst, WHSV = 44.9 h^{-1}, $n(H_2)$:$n(C_3H_8)$ = 0.5:1, 530−560 °C, atmospheric pressure, propane conversion <10%. (i) Results of 24 h PDH on stream, reaction condition: 1.0 g of catalyst, WHSV = 3.04 h^{-1}, $n(H_2)$:$n(C_3H_8)$ = 0.5:1, 600 °C, atmospheric pressure.

H_2:C_3H_8 molar ratio was 0.5:1, WHSV was 2.47 h^{-1}, and the reaction pressure was maintained at 0.3 bar.

The propane conversion is defined as

$$\text{conversion}\ (\%) = \frac{n_{C_3H_8,0} - n_{C_3H_8}}{n_{C_3H_8,0}} \times 100\%$$

where $n_{C_3H_8,0}$ and $n_{C_3H_8}$ are the inlet and outlet molar contents of propane.

The selectivity to propylene is defined as

$$\text{selectivity}\ (\%) = \frac{n_{C_3H_6}}{n_{C_3H_8,0} - n_{C_3H_8}} \times 100\%$$

where $n_{C_3H_6}$ is the molar content of propene at the outlet of the reactor.

The deactivation constant (k_d) is defined as

$$k_d = \frac{\ln[(1 - X_{final}) \div X_{final}] - \ln[(1 - X_{initial}) \div X_{initial}]}{t}$$

where $X_{initial}$ and X_{final} represent the conversion measured at the start and the end of an experiment, and t represents the reaction time (h). Higher k_d values indicate the trend of rapid deactivation, which means low stability.

The apparent activation energy (E_a) was determined by Arrhenius plots below 10% propane conversion at 530−560 °C.

3. RESULTS AND DISCUSSION

The catalysts in the present work were synthesized through the incipient-wetness impregnation method using spherical alumina as support, and the experimental details are described in the Supporting Information (SI). The actual Pt loading of the B-doped catalyst (PtSnK-B0.32) is 0.15 wt %, which is nearly half of that used in industrial catalysts, and the loading of B is 0.32 wt % (Table S1). The Sn and K contents are 0.15 and 0.65 wt %, respectively, as calculated from the theoretical dosages during impregnation. The EDX mapping spectra in Figure S1 illustrate the uniformly dispersed supporting elements in PtSnK-B0.32. PtSnK catalyst, without B doping, was synthesized using the same method and support for comparison. The as-calcined PtSnK-B0.32 and PtSnK show solely diffraction peaks of θ-Al_2O_3 (JCPDS: 23−1009, Figure S2), suggesting the high dispersion of supported components. Their similar N_2 physisorption isotherms and corresponding physical parameters (Figure S3 and Table S2) indicate that trace B doping does not change the textural structures of the catalysts. The aberration-correction high-angle annular dark-field scanning transmission electron microscopy (AC-HAADF-STEM) images in Figure 1a,b declare uniformly dispersed Pt single atoms on both as-calcined PtSnK and PtSnK-B0.32, which are calcined in air at 520 °C for 4 h. After reduction under pure H_2 flow at 600 °C for 2 h, obvious sintering of Pt species occurs on both PtSnK and PtSnK-B0.32 (Figure 1c,d). However, Pt dispersions on these two as-reduced catalysts are apparently different. On as-reduced PtSnK (Figures 1c and S4), the Pt species mainly present as nanoparticles (larger than 2 nm) and nanoclusters (0.5−2 nm) as well as few Pt single atoms. Besides, the Pt nanoparticles on PtSnK show distinct outlines and a crystallized structure of the Pt (111) facet with a crystal lattice of 0.226 nm (Figure 1c,e), indicating the tightly stacked Pt atoms. After B doping, the sizes of Pt species on reduced PtSnK-B0.32 (Figures 1d and S5) dramatically declined, and only Pt nanoclusters smaller than 2 nm and Pt

https://doi.org/10.1021/acscatal.4c07243
ACS Catal. 2025, 15, 4251−4258

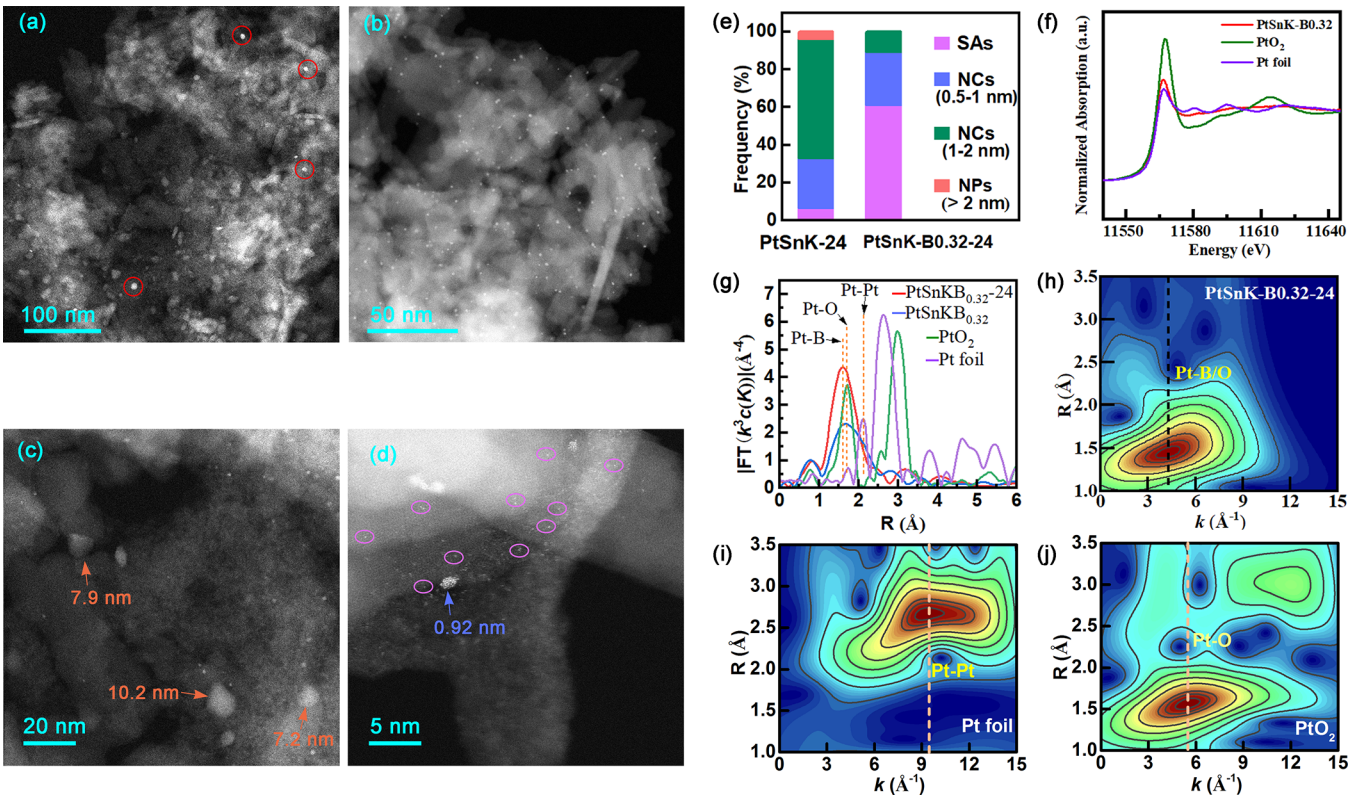

Figure 2. AC-HAADF-STEM images of catalysts after PDH for 24 h (a, c: PtSnK-24; b, d: PtSnK-B0.32−24). (e) Histogram of size distribution of Pt species for PtSnK and PtSnK-B0.32 after 24 h of PDH on stream. (f) The normalized XANES spectra at the Pt L_{III}-edge of PtSnK-B0.32, Pt foil, and PtO_2. (g) Fourier transform of k_3-weighted EXAFS fitting curves of Pt in *R* space. WT-EXAFS plots for PtSnK-B0.32 (h), Pt foil (i), and PtO_2 (j).

single atoms are observed. These nanoclusters on PtSnK-B0.32 have fuzzy outlines and disordered structures (Figure 1d,e), suggesting loosely arranged Pt atoms. Notably, the density of isolated Pt single atoms (signed by purple ovals in Figure 1c,d) on PtSnK-B0.32 is obviously higher compared with that on PtSnK. A more visualized histogram of frequency for Pt species with more than 200 counts for each catalyst is presented in Figure 1f. In detail, the frequency of Pt single atoms on as-reduced PtSnK and PtSnK-B0.32 are 15.8 and 37.8%, respectively. The in situ CO diffuse reflectance infrared Fourier transform spectra (CO−DRIFTS) of reduced PtSnK-B0.32 display three strong peaks at 2075, 2085, and 2123 cm^{-1} (Figure 1g), ascribing to vibration of CO linearly bonded to Pt clusters, metallic Pt single atoms (Pt_1^0), and single ions ($Pt_1^{\delta+}$), respectively.[10,22] The intensified peaks at 2085 and 2123 cm^{-1} declare the high dispersion of Pt species on reduced PtSnK-B0.32. In comparison, these two vibration peaks on reduced PtSnK are much weaker, indicating lower Pt dispersion, which is consistent with AC-HAADF-STEM results. Therefore, trace B doping significantly inhibits the Pt sintering under a high-temperature H_2 reduction process. The H_2 temperature-programmed reduction (H_2-TPR) curve of PtSnK (Figure S6) shows three weak H_2 consumption peaks at 196, 283.1, and 398.2 °C ascribing to the reduction of PtO_2, $PtOCl_2$, and SnO_x, respectively.[12,23,24] The strong signal peak at 626.4 °C (higher than the calcination temperature of the catalyst) might be attributed to the decomposition of chlorine-containing components or dehydration of oxygen-containing groups. After doping of B, H_2 consumption peaks of PtSnK-B0.32 shift to lower temperatures, demonstrating that the incorporation of boron improves the reducibility and electron density of Pt and Sn species.[24]

The PDH performance of the catalysts is initially evaluated in a quartz fixed-bed reactor under atmospheric pressure. The apparent activation energy (E_a) of the catalysts are obtained by plotting ln(TOF) versus $1/T$ (Figure 1h) with propane conversion lower than 10%. The calculated E_a for PtSnK is 84.1 kJ mol^{-1}, which is close to the reported values (80−100 kJ mol^{-1}).[25] After B doping, the E_a value of PtSnK-B0.32 decreases to 63.9 kJ mol^{-1}, which demonstrates that B doping enhances the intrinsic activity of the low-Pt catalyst for PDH reaction. The beneficial effect probably results from the improved electron density and dispersion of Pt species in PtSnK-B0.32.

Then, a 24 h PDH on stream performance of catalysts was investigated at 600 °C with weight hourly space velocity (WHSV) of 3.04 h^{-1} (Figure 1i). PtSnK-B0.32 shows an initial propane conversion of 38.4% and propylene selectivity of 89.0%. Methane (3.81%), ethane (6.45%), and ethylene (0.74%) are the top three byproducts due to hydrocracking of propane or propylene. After reaction for 24 h, the propane conversion on PtSnK-B0.32 slightly decreases to 35.7% and propylene selectivity increases to 91.8%, showing benign durability. PtSnK shows a comparable initial conversion (38.9%) and propylene selectivity (88.4%) to PtSnK-B0.32; however, its conversion after 24 h of reaction is only 32.5%. The deactivation rate (k_d) on PtSnK-B0.32 calculated by the *pseudo-first-order* kinetic model is 0.0049 h^{-1}, which is much lower than that on PtSnK (0.0117 h^{-1}).[16] Besides, the k_d on PtSnK-B0.32 is also lower than most of the Pt-based catalysts

https://doi.org/10.1021/acscatal.4c07243
ACS Catal. 2025, 15, 4251−4258

Table 1. EXAFS Fitting Parameters at the Pt L_3-Edge for Various Samples (S_0^2 = 0.816)[d]

sample	shell	CN[a]	R (Å)[b]	ΔE_0 (eV)[c]	R factor
Pt foil	Pt−Pt	12*	2.76 ± 0.01	7.9 ± 0.3	0.0022
PtO_2	Pt−O	5.8 ± 0.3	2.01 ± 0.01	12.1 ± 0.5	0.0095
	Pt−Pt	6.4 ± 0.6	3.10 ± 0.01		
	Pt−O	8.0 ± 0.4	3.66 ± 0.01		
PtSnK-B0.32	Pt−B	2.2 ± 0.1	2.09 ± 0.01	2.1 ± 1.2	0.0026
	Pt−Pt	4.6 ± 0.4	2.65 ± 0.01		
PtSnK-B0.32−24	Pt−B	1.1 ± 0.3	2.35 ± 0.02	11.7 ± 3.4	0.0005
	Pt−O	3.3 ± 0.9	2.01 ± 0.02		

[a]CN, coordination number. [b]R, distance between absorber and backscatter atoms. [c]ΔE_0, inner potential correction; R factor indicates the goodness of the fit. [d]ΔS_0^2 was fixed as 0.816.

reported in the last five years (Table S3), especially those with Pt loading lower than 0.3 wt %.[3,20,21] In addition, excellent activity and durability are observed for PtSnK-B0.32 at higher WHSV (10.6 and 21.2 h^{-1}, Figures S7 and S8) or higher propane conversion (enhanced reaction equilibrium by N_2 dilution, molar ratio of H_2:C_3H_8:N_2 = 0.5:1:4, Figure S9). These results demonstrate that the B doping significantly enhances the PDH performance of low-Pt catalysts.

Furthermore, catalysts with varied B contents of 0.13 and 0.55% were synthesized, and their reaction performance is displayed in Figure S10. With B loading of 0.13%, the initial propane conversion over PtSnK-B0.13 is 38.8%, which is close to that of PtSnK. After 24 h of reaction, the final propane conversion over PtSnK-B0.13 is 33.8%, which is slightly higher than that of PtSnK, despite the relatively low B/Pt atomic ratio (15:1). This evidences the beneficial effect of B doping on catalyst stability. When the B loading increases to 0.32% (B/Pt atomic ratio is about 30:1), the catalyst stability is significantly enhanced, which has been discussed above. However, as the B loading is further increased to 0.55 wt % (B/Pt atomic ratio is about 65:1), a noticeable decrease in activity is observed without any decline in selectivity. This might be ascribed to the partial covering of Pt species by excess B atoms. Therefore, a suitable content of B is necessary to achieve high performance for low-Pt catalysts.

After 24 h of PDH, Pt species on PtSnK-24 are mainly detected as nanoclusters larger than 1 nm and even some newly formed particles larger than 10 nm (Figures 2a,c and S11), which indicates severe Pt aggregation during 24 h of PDH reaction. This is in accord with previous reports.[1] On the contrary, a distinct diminishment of Pt species is observed on PtSnK-B0.32−24 (Figure 2b,d), where only Pt single atoms and nanoclusters smaller than 1 nm are detected, showing benign aggregation resistance. Notably, the Pt nanoclusters on PtSnK-B0.32−24 remain loosely and disorderly arranged, which indicates a high dispersion of Pt species on PtSnK-B0.32−24. The size distribution of Pt species shown in Figure 2e reveals that the frequency of Pt single atoms on PtSnK-24 is reduced from 15.8% (as-reduced PtSnK in Figure 1f) to 6.7%. However, a completely opposite trend is observed for PtSnK-B0.32−24, where the statistical frequency of Pt single atoms increased to 61.1%, which is much higher than that on as-reduced PtSnK-B0.32 (37.8%, Figure 1f). Even after 90 h on stream, 25.0% of Pt single atoms are still retained without large nanoparticles (>2 nm) on PtSnK-B0.32−90 (Figure S12). Note that the ICP analysis (Table S4) shows a small Pt loss during the PDH process. Obviously, Pt species on PtSnK-B0.32 are redispersed during the PDH reaction.

The normalized X-ray absorption near-edge structure (XANES) spectra (Figure 2f) show a much lower near-edge absorption energy for as-reduced PtSnK-B0.32 than that for PtO_2 but slightly higher than that for Pt foil, suggesting a mainly metallic state of Pt atoms. XAS spectra of as-reduced PtSnK-B0.32 show a primary signal at 1.65 Å (no phase correction, Figures 2g and S13), slightly lower than that of PtO_2 at 1.8 Å (Pt−O), ascribing to the partial coordination of Pt with B atoms.[26] The negative shift of the k value of WT-EXAFS for as-reduced PtSnK-B0.32 (Figure 2h) in comparison with Pt foil (Figure 2i) and PtO_2 (Figure 2j) further confirms the formation of Pt−B bonds. Additionally, the Pt−B bond is also verified by the XANES spectra of B K-edge in Figure S14, where a slight shift to higher energy of B K-edge is observed on PtSnK-B0.32 in comparison with that of 0.35 wt %B/Al_2O_3. The deconvolution curves displayed mainly four peaks for B 1s. The B 1s XPS spectrum of reduced PtSnK-B0.32 (Figure S15) displayed four peaks for B 1s. The peak at 191.1 eV is attributed to elemental boron (B^0 or Pt−B^0), and the other three peaks at higher binding energies (192.1, 193.0, and 194.1 eV) are attributed to a boron suboxide and B_2O_3 for PtSnK-B0.32.[27] Meanwhile, a weak feature attributed to Pt−Pt bonds (Pt foil, 2.10 Å) is also observed on as-reduced PtSnK-B0.32 (Figure 2g), indicating a small amount of Pt clusters on reduced PtSnK-B0.32, consistent with the AC-HAADF-STEM results (Figure 1d). The R-space and K-space EXAFS fitting analysis (Figure 2g and Table 1) display that the coordination number (CN) of Pt−Pt and Pt−B for as-reduced PtSnK-B0.32 are ∼4.6 and ∼2.2, respectively. After PDH for 24 h, the Pt−Pt bond on PtSnK-B0.32−24 totally disappeared, which confirms the redispersion of Pt species during PDH.[16,21] The presence of the Pt−O bond in PtSnK-B0.32−24 may be ascribed to the partial oxidation of highly dispersed Pt species as it is exposed to air during sampling.

Considering that Pt sintering indeed occurs on both PtSnK and PtSnK-B0.32 during the H_2 reduction process as displayed in Figure 1c,d, the redispersion of Pt species during the PDH reaction is reasonably speculated to be initiated by propane molecules. To prove this hypothesis, as-calcined PtSnK-B0.32 was further reduced under pure H_2 flow (without propane) for 24 h at the same temperature (600 °C) as PDH. As expected, large Pt nanoparticles with sizes of 5−10 nm are generated (Figure S16), which, however, did not appear on PtSnK-B0.32−24 after 24 h of PDH on stream. The coking deposit can be excluded from helping Pt redispersion as the sizes of Pt species on PtSnK-B0.32−90 are slightly larger than those on PtSnK-B0.32−24 despite its much higher coke content (PtSnK-B0.32−90:4.51 wt % vs PtSnK-B0.32−24:2.12 wt %). The possible mechanism is as follows: at the initial PDH

https://doi.org/10.1021/acscatal.4c07243
ACS Catal. 2025, 15, 4251−4258

stage, propane molecules contact well with Pt species to maintain their redispersion. However, with the proceeding of PDH, increasing coke formation on PtSnK-B0.32 covers the Pt species, preventing their access to propane molecules, which induces deactivation of catalysts and impedes redispersion of Pt clusters. As a result, an extremely slow aggregation of Pt species proceeds again. It should also be noted that no redispersion phenomenon of Pt species is observed on PtSnK during PDH, so the doped B is another essential prerequisite for Pt redispersion.

To elucidate how B species promote the Pt redispersion process on B-doped catalyst, theoretical DFT calculations were further performed. Based on the Pt−B structure derived from XAS, two of the most possible Pt−B cluster models (Pt_6B_1 and Pt_6B_2) were proposed and the binding energies of Pt−B clusters and pure Pt cluster (Pt_6) on the (010) surface of θ-Al_2O_3 are simulated. Notably, the molar ratio of Pt to B calculated by DFT is based on the results of synchrotron radiation, which also indicates that only a portion of boron will bond with platinum. On PtSnK-B0.32, B atoms are in excess with a B/Pt atomic ratio of approximately 30:1, so most B atoms have no access to Pt atoms. The Pt_6B_1 and Pt_6B_2 models used here are likely the most possible and typical models according to synchrotron radiation results. The optimized lowest-energy structure and corresponding binding energy of three Pt(-B) cluster models are shown in Figure 3a and Table S5. Notably, PtSnK and PtSnK-B0.32 have the same loading of Pt (0.14−0.15 wt %), Sn (0.1 wt %), and K (0.65 wt %), and the sole difference between them is whether B is doped. Thus, the significant difference of catalytic performance between PtSnK and PtSnK-B0.32 is undoubtably caused by B. Moreover, Sn and K are not directly bonding to Pt or B species according to synchrotron radiation and aberration electron microscopy results. Therefore, for simplicity and to clearly demonstrate the structure of Pt−B clusters, DFT models in Figure 3a show only Pt and B atoms, where Sn and K are hided. The calculated binding energies of Pt_6, P_6B_1, and Pt_6B_2 on the θ-Al_2O_3(010) surface are −7.40, −9.42, and −11.16 eV, respectively. The binding energies of Pt−B clusters on the Al_2O_3(010) surface are much lower (more negative) than that of the pure Pt cluster. Hence, compared with pure Pt clusters, Pt−B clusters are more stable, and Pt sintering is harder to occur.[28] Furthermore, the bonding behavior of the Pt−B cluster is simulated under a propane atmosphere, and the corresponding optimized structure of the critical intermediate is shown in Figures S17 and S18. As shown in Table S6, compared with the Pt_6B_2 cluster (after H_2 activation), the bond lengths between Pt atoms become longer after adsorbing propane, indicating that the propane atmosphere is conducive to the dissociation of Pt atoms, which is consistent with the redispersion of Pt species in the experiment. In other words, when Pt atoms over pure clusters or nanoparticles mobilize on support during PDH, they are readily captured by B or BO_x species to form stable Pt−B clusters and redispersed on support (Figure 3b).

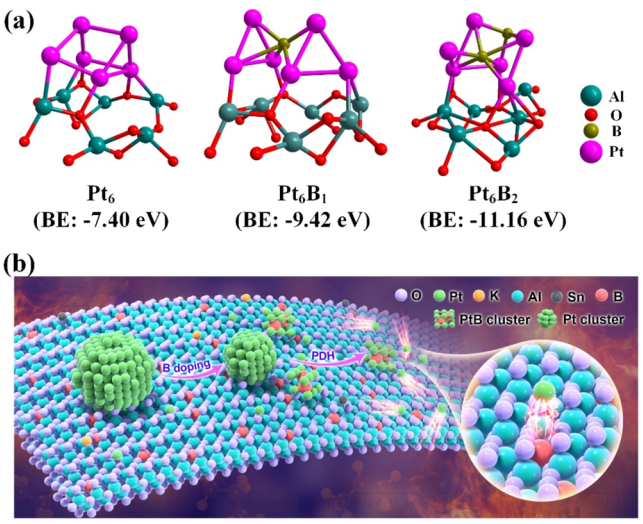

Figure 3. (a) Optimized lowest-energy cluster structures of pure Pt_6, Pt_6B_1, and Pt_6B_2 and their corresponding binding energy on θ-Al_2O_3 (010). Note: For simplicity, K and Sn atoms were hided. (b) Possible redispersion mechanism of Pt species on PtSnK-B0.32.

As discussed above, B-doped catalyst shows excellent aggregation resistance and redispersion capability during the PDH process, so high durability is reasonably expected. Herein, lifetime experiments were further performed on a stainless reactor with a WHSV of 2.47 h^{-1} and a pressure of 0.3 bar. As shown in Figure 4, the propane conversion over PtSnK declines rapidly to lower than 20% after 100 h of reaction. Interestingly, by doping trace amounts of B, the durability of PtSnK-B0.32 is significantly improved. During the initial 120 h, the propane conversion on PtSnK-B0.32 decreases very slowly from 37.1 to 35.1%. Then, a slightly higher deactivation rate is observed, however, which is still much lower than PtSnK. When the conversion falls to 20%, the single-pass lifetime of PtSnK-B0.32 is 310 h, which is three times that of PtSnK. A similar trend is also detected for propylene selectivity, despite the slightly lower values in comparison with results on quartz reactor due to the severe hydrocracking under higher pressure and catalytic coking on the inner walls of stainless-steel reactor.

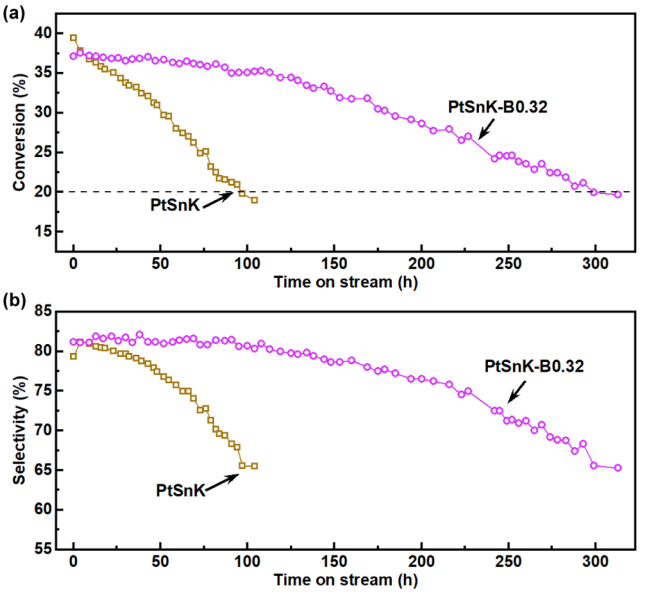

Figure 4. Propane conversion (a) and propylene selectivity (b) of lifetime experiments of PDH on PtSnK-B0.32 and PtSnK, reaction condition: 6.0 g catalyst, WHSV = 2.47 h^{-1}, $n(H_2)$:$n(C_3H_8)$ = 0.5:1, 600 °C, 0.3 bar.

To further certify the high durability and practical application feasibility of PtSnK-B0.32, a B-free Pt−Sn−K/

https://doi.org/10.1021/acscatal.4c07243
ACS Catal. 2025, 15, 4251−4258

Al_2O_3 catalyst with Pt loading of 0.26 wt % (referred to as 0.26PtSnK), similar to the industrial catalyst used by UOP, is also synthesized for comparison. Under the same PDH conditions, the single-pass lifetime of 0.26PtSnK is 142 h when propane conversion falls to 20% (Figure S19), which is less than half of that of PtSnK-B0.32 despite its much higher Pt content. High durability of catalyst means lower regeneration frequency and lower Pt loading signifies less catalyst cost. More importantly, our B-doped catalyst facilely derives from conventional Pt−Sn−K/Al_2O_3-based PDH catalysts, which complies with the operation conditions of existing PDH plants of the Oleflex process and can be directly adopted without plant remolding or new construction. This explicitly illustrates the promising industrial application perspective of our low-Pt catalyst.

4. CONCLUSIONS

In summary, a low-Pt (0.15 wt %) catalyst with excellent PDH catalytic activity and durability is synthesized through the facile doping of B into conventional Pt-based catalysts. The introduction of B species can remarkably promote the catalytic performance of Pt clusters through the formation of highly dispersed Pt−B clusters. The PtSnK-B0.32 catalyst exhibits extremely high durability, with a single-pass lifetime three times that of PtSnK and twice that of 0.26PtSnK (0.26 wt % Pt) under the same conditions. Moreover, outstanding activity and durability are observed over PtSnK-B0.32 at higher WHSV (10.6 and 21.2 h^{-1}) or higher propane conversion (enhanced reaction equilibrium by N_2 dilution). The characterization results show that trace B doping significantly inhibits Pt sintering during the high-temperature H_2 reduction process. Significantly, when propane molecules are adsorbed on the B-doped catalyst, the bond lengths between Pt atoms become longer and dissociation of Pt atoms gets easier. The dissociated Pt atoms are readily captured by B or BO_x species to form stable Pt−B clusters, resulting in the redispersion of Pt species on the B-doped catalyst during the reaction process. This work sheds new light on the design of catalysts with both low Pt loading and high PDH performance.

■ ASSOCIATED CONTENT

Data Availability Statement

All data needed to evaluate the conclusions in the paper are present in the paper or the Supporting Information.

Supporting Information

The Supporting Information is available free of charge at https://pubs.acs.org/doi/10.1021/acscatal.4c07243.

Detailed information on the catalytic performance of PDH over Pt-based catalysts, comparison of catalytic performance of reported platinum-based catalysts for PDH; EDX mapping spectra of PtSnK-B0.32; XRD patterns, N_2 isotherms, AC-HAADF-STEM images, and H_2-TPR curves for fresh catalysts; PDH performance over Pt-based catalysts with WHSV = 10.6/21.2 h^{-1}, N_2 balance, and different B loadings; AC-HAADF-STEM images of used catalysts; ICP analysis results of fresh and used catalysts; EXAFS fitting curves of fresh and used PtSnK-B0.32; XANES of the B K-edge of PtSnK-B0.32; optimized structures of Pt_6B_2−Cluster; PDH performance over 0.26PtSnK (Figures S1−S8) (Tables S1−S6) (PDF)

■ AUTHOR INFORMATION

Corresponding Authors

Bin Gu − *Dalian Institute of Chemical Physics, Chinese Academy of Sciences, Dalian 116023 Liaoning, China;* orcid.org/0000-0002-1427-4489; Email: gubinseven12@dicp.ac.cn

Chenglin Sun − *Dalian Institute of Chemical Physics, Chinese Academy of Sciences, Dalian 116023 Liaoning, China;* Email: clsun@dicp.ac.cn

Authors

Mengyang Liu − *Dalian Institute of Chemical Physics, Chinese Academy of Sciences, Dalian 116023 Liaoning, China; SINOPEC (Dalian) Research Institute of Petroleum and Petrochemical Co., Ltd., Dalian 116045 Liaoning, China; University of Chinese Academy of Sciences, Beijing 100049, China*

Shaobo Han − *Dalian Institute of Chemical Physics, Chinese Academy of Sciences, Dalian 116023 Liaoning, China*

Wenna Zhang − *Dalian Institute of Chemical Physics, Chinese Academy of Sciences, Dalian 116023 Liaoning, China*

Jingmei Li − *Dalian Institute of Chemical Physics, Chinese Academy of Sciences, Dalian 116023 Liaoning, China*

Huangzhao Wei − *Dalian Institute of Chemical Physics, Chinese Academy of Sciences, Dalian 116023 Liaoning, China;* orcid.org/0000-0002-9370-9240

Xin Rong − *Dalian Institute of Chemical Physics, Chinese Academy of Sciences, Dalian 116023 Liaoning, China*

Complete contact information is available at: https://pubs.acs.org/10.1021/acscatal.4c07243

Author Contributions

‖M.L., S.H., and W.Z. contributed equally to this work. The manuscript was written through the contributions of all authors. All authors have given approval to the final version of the manuscript.

Funding

This work was financially supported by the National Natural Science Foundation of China (No. 21802135), the CNPC-DICP Joint Research Center, and the Youth Innovation Promotion Association CAS (2020190).

Notes

The authors declare no competing financial interest.

■ REFERENCES

(1) Sattler, J. J. H. B.; Ruiz-Martinez, J.; Santillan-Jimenez, E.; Weckhuysen, B. M. Catalytic Dehydrogenation of Light Alkanes on Metals and Metal Oxides. *Chem. Rev.* **2014**, *114* (20), 10613−10653.

(2) Ryoo, R.; Kim, J.; Jo, C.; Han, S. W.; Kim, J. C.; Park, H.; Han, J.; Shin, H. S.; Shin, J. W. Rare-earth-platinum alloy nanoparticles in mesoporous zeolite for catalysis. *Nature* **2020**, *585* (7824), 221−224.

(3) Wang, P.; Yao, J.; Jiang, Q.; Gao, X.; Lin, D.; Yang, H.; Wu, L.; Tang, Y.; Tan, L. Stabilizing the isolated Pt sites on PtGa/Al_2O_3 catalyst via silica coating layers for propane dehydrogenation at low temperature. *Appl. Catal., B* **2022**, *300*, No. 120731.

(4) Atanga, M. A.; Rezaei, F.; Jawad, A.; Fitch, M.; Rownaghi, A. A. Oxidative dehydrogenation of propane to propylene with carbon dioxide. *Appl. Catal., B* **2018**, *220*, 429−445.

(5) Dai, Y.; Gu, J.; Tian, S.; Wu, Y.; Chen, J.; Li, F.; Du, Y.; Peng, L.; Ding, W.; Yang, Y. gamma-Al_2O_3 sheet-stabilized isolate Co^{2+} for catalytic propane dehydrogenation. *J. Catal.* **2020**, *381*, 482−492.

(6) Sattler, J. J. H. B.; Gonzalez-Jimenez, I. D.; Luo, L.; Stears, B. A.; Malek, A.; Barton, D. G.; Kilos, B. A.; Kaminsky, M. P.; Verhoeven, T. W. G. M.; Koers, E. J.; Baldus, M.; Weckhuysen, B. M. Platinum-

Promoted Ga/Al_2O_3 as Highly Active, Selective, and Stable Catalyst for the Dehydrogenation of Propane. *Angew. Chem., Int. Ed.* **2014**, *53* (35), 9251−9256.
(7) Im, J.; Choi, M. Physicochemical Stabilization of Pt against Sintering for a Dehydrogenation Catalyst with High Activity, Selectivity, and Durability. *ACS Catal.* **2016**, *6* (5), 2819−2826.
(8) Xiong, H.; Lin, S.; Goetze, J.; Pletcher, P.; Guo, H.; Kovarik, L.; Artyushkova, K.; Weckhuysen, B. M.; Datye, A. K. Thermally Stable and Regenerable Platinum-Tin Clusters for Propane Dehydrogenation Prepared by Atom Trapping on Ceria. *Angew. Chem., Int. Ed.* **2017**, *56* (31), 8986−8991.
(9) Monzon, A.; Garetto, T. F.; Borgna, A. Sintering and redispersion of Pt/gamma-Al_2O_3 catalysts: a kinetic model. *Appl. Catal., A* **2003**, *248* (1−2), 279−289.
(10) Han, B.; Guo, Y.; Huang, Y.; Xi, W.; Xu, J.; Luo, J.; Qi, H.; Ren, Y.; Liu, X.; Qiao, B.; Zhang, T. Strong Metal-Support Interactions between Pt Single Atoms and TiO_2. *Angew. Chem., Int. Ed.* **2020**, *59* (29), 11824−11829.
(11) Liu, S.; Qi, H.; Zhou, J.; Xu, W.; Niu, Y.; Zhang, B.; Zhao, Y.; Liu, W.; Ao, Z.; Kuang, Z.; Li, L.; Wang, M.; Wang, J. Encapsulation of Platinum by Titania under an Oxidative Atmosphere: Contrary to Classical Strong Metal-Support Interactions. *ACS Catal.* **2021**, *11* (10), 6081−6090.
(12) Shi, L.; Deng, G.-M.; Li, W.-C.; Miao, S.; Wang, Q.-N.; Zhang, W.-P.; Lu, A.-H. Al_2O_3 Nanosheets Rich in Pentacoordinate Al^{3+} Ions Stabilize Pt-Sn Clusters for Propane Dehydrogenation. *Angew. Chem., Int. Ed.* **2015**, *54* (47), 13994−13998.
(13) Li, X.; Pereira-Hernandez, X. I.; Chen, Y.; Xu, J.; Zhao, J.; Pao, C.-W.; Fang, C.-Y.; Zeng, J.; Wang, Y.; Gates, B. C.; Liu, J. Functional CeO_x nanoglues for robust atomically dispersed catalysts. *Nature* **2022**, *611* (7935), 284−288.
(14) Pham, H. N.; Sattler, J. J. H. B.; Weckhuysen, B. M.; Datye, A. K. Role of Sn in the Regeneration of Pt/gamma-Al_2O_3 Light Alkane Dehydrogenation Catalysts. *ACS Catal.* **2016**, *6* (4), 2257−2264.
(15) Chen, S.; Zhao, Z.-J.; Mu, R.; Chang, X.; Luo, J.; Purdy, S. C.; Kropf, A. J.; Sun, G.; Pei, C.; Miller, J. T.; Zhou, X.; Vovk, E.; Yang, Y.; Gong, J. Propane Dehydrogenation on Single-Site [$PtZn_4$] Intermetallic Catalysts. *Chem* **2021**, *7* (2), 387−405.
(16) Sun, Q.; Wang, N.; Fan, Q.; Zeng, L.; Mayoral, A.; Miao, S.; Yang, R.; Jiang, Z.; Zhou, W.; Zhang, J.; Zhang, T.; Xu, J.; Zhang, P.; Cheng, J.; Yang, D.-C.; Jia, R.; Li, L.; Zhang, Q.; Wang, Y.; Terasaki, O.; Yu, J. Subnanometer Bimetallic Platinum-Zinc Clusters in Zeolites for Propane Dehydrogenation. *Angew. Chem., Int. Ed.* **2020**, *59* (44), 19450−19459.
(17) Wang, T.; Jiang, F.; Liu, G.; Zeng, L.; Zhao, Z.-j.; Gong, J. Effects of Ga doping on Pt/CeO_2-Al_2O_3 catalysts for propane dehydrogenation. *AlChE J.* **2016**, *62* (12), 4365−4376.
(18) Yan, H.; He, K.; Samek, I. A.; Jing, D.; Nanda, M. G.; Stair, P. C.; Notestein, J. M. Tandem In_2O_3-Pt/Al_2O_3 catalyst for coupling of propane dehydrogenation to selective H_2 combustion. *Science* **2021**, *371* (6535), 1257−1260.
(19) Escorcia, N. J.; LiBretto, N. J.; Miller, J. T.; Li, C. W. Colloidal Synthesis of Well-Defined Bimetallic Nanoparticles for Nonoxidative Alkane Dehydrogenation. *ACS Catal.* **2020**, *10* (17), 9813−9823.
(20) Sun, G.; Zhao, Z.-J.; Mu, R.; Zha, S.; Li, L.; Chen, S.; Zang, K.; Luo, J.; Li, Z.; Purdy, S. C.; Kropf, A. J.; Miller, J. T.; Zeng, L.; Gong, J. Breaking the scaling relationship via thermally stable Pt/Cu single atom alloys for catalytic dehydrogenation. *Nat. Commun.* **2018**, *9*, No. 4454.
(21) Liu, G.; Zeng, L.; Zhao, Z.-J.; Tian, H.; Wu, T.; Gong, J. Platinum-Modified ZnO/Al_2O_3 for Propane Dehydrogenation: Minimized Platinum Usage and Improved Catalytic Stability. *ACS Catal.* **2016**, *6* (4), 2158−2162.
(22) Qiao, B.; Wang, A.; Yang, X.; Allard, L. F.; Jiang, Z.; Cui, Y.; Liu, J.; Li, J.; Zhang, T. Single-atom catalysis of CO oxidation using Pt-1/FeO_x. *Nat. Chem.* **2011**, *3* (8), 634−641.
(23) Luo, S.; Wu, N.; Zhou, B.; He, S.; Qiu, J.; Sun, C. Effect of alumina support on the performance of Pt-Sn-K/gamma-Al_2O_3 catalyst in the dehydrogenation of isobutane. *J. Fuel Chem. Technol.* **2013**, *41* (12), 1481−1487.
(24) Liu, X.; Lang, W.-Z.; Long, L.-L.; Hu, C.-L.; Chu, L.-F.; Guo, Y.-J. Improved catalytic performance in propane dehydrogenation of PtSn/gamma-Al_2O_3 catalysts by doping indium. *Chem. Eng. J.* **2014**, *247*, 183−192.
(25) Ma, R.; Yang, T.; Gao, J.; Kou, J.; Chen, J. Z.; He, Y.; Miller, J. T.; Li, D. Composition Tuning of Ru-Based Phosphide for Enhanced Propane Selective Dehydrogenation. *ACS Catal.* **2020**, *10* (17), 10243−10252.
(26) Gu, Y.; Wang, S.; Shi, H.; Yang, J.; Li, S.; Zheng, H.; Jiang, W.; Liu, J.; Zhong, X.; Wang, J. Atomic Pt Embedded in BNC Nanotubes for Enhanced Electrochemical Ozone Production via an Oxygen Intermediate-Rich Local Environment. *ACS Catal.* **2021**, *11* (9), 5438−5451.
(27) Ong, C. W.; Huang, H.; Zheng, B.; Kwok, W. M. R.; Hui, Y. Y.; Lau, M. W. X-ray photoemission spectroscopy of nonmetallic materials: Electronic structures of boron and B_xO_y. *J. Appl. Phys.* **2004**, *95* (7), 3527−3534.
(28) Dadras, J.; Jimenez-Izal, E.; Alexandrova, A. N. Alloying Pt Subnano-clusters with Boron: Sintering Preventative and Coke Antagonist? *ACS Catal.* **2015**, *5* (10), 5719−5727.

https://doi.org/10.1021/acscatal.4c07243
ACS Catal. 2025, 15, 4251−4258